

On the Fraction of Internal Tide Energy Dissipated Near Topography

Louis C. St. Laurent

Department of Oceanography, Florida State University, Tallahassee, Florida

Jonathan D. Nash

College of Oceanic and Atmospheric Science, Oregon State University, Corvallis, Oregon

Abstract. Internal tides have been implicated as a major source of mechanical energy for mixing in the ocean interior. Indeed, microstructure and tracer measurements have indicated that enhanced turbulence levels occur near topography where internal tides are generated. However, the details of the energy budget and the mechanisms by which energy is transferred from the internal tide to turbulence have been uncertain. It now seems that the energy levels associated with locally enhanced mixing near topography may constitute only a small fraction of the available internal tide energy flux.

In this study, the generation, radiation, and energy dissipation of deep ocean internal tides are examined. Properties of the internal tide at the Mid-Atlantic Ridge and Hawaiian Ridge are considered. It is found that most internal tide energy is generated as low modes. The Richardson number of the generated internal tide typically exceeds unity for these motions, so direct shear instability of the generated waves is not the dominant energy transfer mechanism. It also seems that wave-wave interactions are ineffective at transferring energy from the large wavelengths that dominate the energy flux. Instead, it seems that much of the generated energy radiates away from the generation site in low mode waves. These low modes must dissipate somewhere in the ocean, though this likely occurs over $O(1000 \text{ km})$ distances as the waves propagate. Additionally, a small fraction of energy flux is generated as high mode waves. These have slower group speeds, higher shear, and faster wave-wave interaction rates than the low modes, and so are likely to dissipate as turbulence close to the topography of the generation site. Preliminary estimates suggest that turbulent dissipation near sites of generation accounts for 30% or less of the total generated energy flux. Based on these estimates, a parameterization of the mixing sustained by high mode internal tide generation is proposed.

1. Introduction

Breaking internal waves are the main cause of diapycnal mixing in the ocean's interior. They may be generated by wind at the sea surface or by flow over the topography of the seafloor. While mean flows and eddy activity in the deep ocean are characterized by $O(1) \text{ mm s}^{-1}$ currents, deep barotropic tidal currents are $O(10) \text{ mm s}^{-1}$ and may be an important source of internal waves. Recent studies (*Munk and Wunsch,*

1998; Egbert and Ray, 2000; 2001; Jayne and St. Laurent, 2001) have implicated the internal tides as a major source of mechanical energy for mixing, providing up to 1 TW of power to the deep ocean. While some studies suggest this amount of energy is sufficient for powering the mixing that closes the meridional overturning cell of the ocean's thermohaline circulation (*Webb and Sugimotohara, 2001*), other studies suggest that internal tides provide only half of the needed energy (*Munk and Wunsch,*

sch, 1998). Wind forcing may also supply a significant fraction of the energy input to the internal wavefield through the generation of *near-inertial swell* (Alford, 2001, 2003a). This highlights the need for studies to examine the relative contributions from each of these sources to internal waves and mixing.

Egbert and Ray (2000, 2001) have identified a number of deep ocean regions where barotropic tidal energy is likely being transferred to internal tides. These regions are generally associated with three types of topography: (i) oceanic islands, (ii) oceanic trenches, and (iii) mid-ocean ridges. Oceanic islands such as Hawaii, and oceanic trenches such as those in the west Pacific Ocean, are steep topographic features with typical slopes (s ; rise over run) of 0.1 to 0.3 (*Seibold and Berger*, 1996). *Egbert and Ray* (2000, 2001) identify the oceanic islands of Micronesia and Melanesia as sites accounting for over 100 GW of internal tide production, while Hawaii accounts for 20 GW. They also identify mid-ocean ridge topography in the Atlantic and Indian Oceans as each accounting for over 100 GW of internal tide production. These topographic features have slopes that vary over a wide range of spatial scales.

a. Observations of internal tides and mixing

The contribution of internal tides to oceanic velocity and temperature records has long been recognized. *Wunsch* (1975) and *Hendershott* (1981) present reviews of earlier work. Renewed interest in internal tides came with observations of sea surface elevation by the Topex/Poseidon altimeter. These data have been used to constrain hydrodynamic models of the tides, and hence produce accurate estimates of open-ocean barotropic tides (*Egbert et al.*, 1994; *Egbert*, 1997). A multi-year record of satellite observations is now available, and the semidiurnal tides (M_2 and S_2) can be dealiased from the record. *Ray and Mitchum* (1996) used along-track Topex/Poseidon records to examine the surface manifestation of internal tides generated along the Hawaiian Islands. They found that both first and second baroclinic modes of the semidiurnal internal tides were present in the data, and that the signal of internal-tide propagation could be tracked up to 1000 km away from the Hawaiian Ridge. In a further analysis of the altimetry data, *Ray and Mitchum* (1997) estimate that 15 GW of semidiurnal internal tide energy radiates away from the Hawaiian Ridge in the first baroclinic mode.

Microstructure observations have provided direct observations of mixing driven by internal tides at steep topography (*Lueck and Mudge*, 1997; *Kunze and Toole*, 1997; *Lien and Gregg*, 2001; *Kunze et al.*, 2002a,b; *Althaus et al.*, 2003). *Lueck and Mudge* (1997) attributed

enhanced turbulence at Cobb Seamount in the north-east Pacific to a semidiurnal internal tide. They found that the largest turbulence levels occurred along a beam of internal tide energy emanating from the seamount rim. *Kunze and Toole* (1997) describe microstructure observations from Fieberling Seamount in the north-east Pacific. They found the largest mixing levels at the summit of the seamount where diurnal internal tide energy was trapped. Internal tides are also produced along the continental margins of the ocean basins, and evidence of internal tide driven mixing at Monterey Canyon off California was reported by *Lien and Gregg* (2001) and *Kunze et al.* (2002a). There, enhanced turbulence levels were found along the ray path of a semidiurnal internal tide beam extending out a distance of 4 km away from the topography. *Althaus et al.* (2003) present fine structure observations of internal tides at Mendocino Escarpment. In addition to finding evidence for strong mixing near the topography, they find enhanced mixing at sites where beams of internal tide energy refract beneath the sea surface.

Evidence of internal tide driven mixing from the truly deep ocean was found during the Brazil Basin Tracer Release Experiment (BBTRE; *Polzin et al.*, 1997; *Ledwell et al.*, 2000; *St. Laurent et al.*, 2001). This study was conducted near the Mid-Atlantic Ridge. *St. Laurent et al.* (2001) present vertically integrated dissipation data that are modulated over the spring-neap tidal cycle with a small lag of about a day. Maximum levels of dissipation, vertically integrated to 2000 m above the bottom, reach 3 mW m^{-2} . These observations span a network of fracture zones west of the Mid-Atlantic Ridge, with topographic relief varying by up to 1 km between the crests and floors of abyssal canyons. The dominant topography of the fracture zone system has a slope less than 0.1 as the canyons are generally 30 to 50 km wide. Elevated turbulent dissipation rates were found along all regions of the fracture zone topography, but turbulence levels appeared most enhanced over the slopes. Above all classes of topography, turbulence levels decrease to background levels at heights above bottom greater than about 1000 m.

Observations of deep, tidally driven mixing have also been made as part of the Hawaii Ocean Mixing Experiment (*HOME*; *Pinkel et al.*, 2000). Both near- and far-field observational components were conducted, and fine- and microstructure measurements allowed for estimates of tidal energy flux and turbulent dissipation. Preliminary HOME observations to be reported here were presented by *Kunze et al.* (2002b).

Figure 1 shows turbulent dissipation profiles from several sites where internal tides are believed to support mixing. Average profiles from sites of internal tide

generation include the Mid-Atlantic Ridge of the Brazil Basin (Polzin *et al.*, 1997; Ledwell *et al.*, 2000; St. Laurent *et al.*, 2001), and the 3000-m isobath of the Hawaiian Ridge (Kunze *et al.*, 2002b). The latter was averaged from 16 stations spanning roughly ~ 1000 km along the Hawaiian Ridge. These stations were occupied over a 3-week period during October 2000 and capture energy flux radiated from both strong and weak sites of internal tide generation along the ridge. Profiles from the Oregon Slope (Moum *et al.*, 2002) and the Virginia Slope (Nash *et al.*, 2003) are also shown, as turbulence at these sites is likely supported by dissipating low mode internal tides. At all sites, the dissipation rates are maximum along the topography, and decay away from the topography with height. Enhanced turbulence levels are found to extend up to 1000 m from the bottom.

The energy flux carried by the internal tide can radiate as propagating internal waves, and these waves are subject to a collection of processes that will eventually lead to dissipation. Shear instability, wave-wave interactions, and topographic scattering all act to influence the rate of dissipation and control whether the internal tide dissipates near the generation site or far away. Understanding the physical cascade that allows energy in the internal tide to power turbulence is one goal of ocean mixing research.

2. Internal tide energy flux

Several nondimensional parameters are needed to model the physical regime of internal tide generation. One parameter, kU_0/ω , measures the ratio of the tidal excursion length scale U_0/ω to the length scale of the topography k^{-1} . This parameter is discussed by Bell (1975) and others, and distinguishes a wave response dominated by the fundamental tidal frequency ($kU_0/\omega < 1$) from a lee-wave response involving higher tidal harmonics ($kU_0/\omega > 1$). A second parameter, $\delta = h_0/H$, measures the ratio of the topographic amplitude h_0 to the total depth H . A third parameter, s/α , measures the ratio of the maximum topographic slope $s = |\nabla h|$ to the ray slope given by $\alpha = ((\omega^2 - f^2)/(N^2 - \omega^2))^{1/2}$. This parameter also distinguishes two regimes. In the case of $s/\alpha < 1$, the topographic slopes are less steep than the radiated tidal beam, and internal wave generation is termed subcritical. In the case of $s/\alpha > 1$, the topographic slopes exceed the steepness of the radiated beam and the internal wave generation is termed supercritical. The critical generation condition is met when the radiated tidal beam is aligned with the slope of the topography.

The subcritical generation of internal tides was first considered by Cox and Sandstrom (1962), Baines (1973),

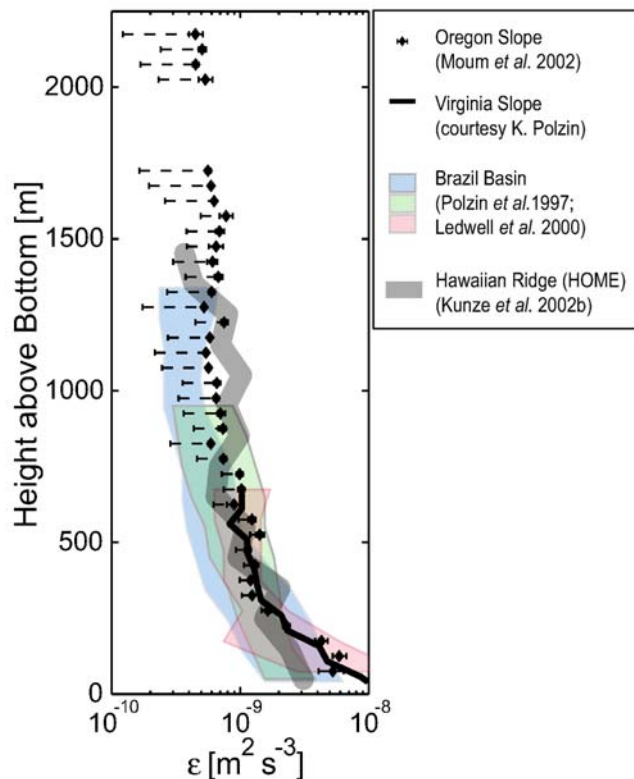


Figure 1. Average profiles of turbulent dissipation from several sites where internal tides support mixing. Oregon Slope data (Moum *et al.*, 2002; shown with 95% confidence intervals) and Virginia Slope data (Nash *et al.*, 2003) show mixing supported by the dissipation of low mode internal tides. The 95% confidence intervals for data from Brazil Basin fracture-zone valleys, crests, and slopes are shown as blue, green, and red shaded bands, respectively, as described by Ledwell *et al.* (2000). Dissipation at the 3000-m isobath of the Hawaiian Ridge was derived from data described in the text.

and Bell (1975). These studies examined subcritical topography in the limit of $\delta \ll 1$ and $s/\alpha \ll 1$, for which the bottom boundary condition can be linearized to $w(-H) = \mathbf{U} \cdot \nabla h$. In this case, the internal tide generation problem can be solved for topography of arbitrary shape by Fourier decomposition. Later studies have examined the initial transient wave response, finite depth effects, depth-varying stratification, and spatial variations in topography and tidal forcing (Hibiya, 1986; Khaliwala, 2003; Li, 2003; Llewellyn Smith and Young, 2002; St. Laurent and Garrett, 2002). Of central interest in all studies is the production of baroclinic energy as the barotropic tide responds to changes in topography. In the limit of small tidal excursion ($kU_0/\omega \ll 1$), the conversion rate is equal to the energy flux (E_f) away from the topography. Llewellyn Smith and Young (2002) show that the energy flux in the limits of $s/\alpha \ll 1$ and $kU_0/\omega \ll 1$ is

$$E_f = E_0 H^{-2} \sum_{n=1}^{\infty} k_n \tilde{h}(k_n) \tilde{h}^*(k_n) \Delta k, \quad (1)$$

where $k_n = n\Delta k = \alpha n\pi/H$ denote the horizontal wavenumbers of the resonant modes and \tilde{h} is the Fourier transform of the topography. Here,

$$E_0 = \frac{1}{2\pi} \rho \frac{((N^2 - \omega^2)(\omega^2 - f^2))^{1/2}}{\omega} U_0^2 H^2 \quad (2)$$

is a convenient metric for the energy flux amplitude, with the rest of (1) being nondimensional. St. Laurent and Garrett (2002) have discussed the representation of (1) using an integral over a continuous spectrum rather than a summation over discrete modes.

Internal tide generation at topography of finite steepness was considered by Baines (1982). In that study, ray tracing methods were developed to permit the full range of δ and s/α . The integral equations derived by Baines (1982) are difficult to apply to arbitrary topography, and Baines did not examine the sensitivity of the conversion rate to the steepness of the topography. Using an approach similar to Baines, Craig (1987) specifically considered a continental slope of finite steepness, but only considered $s/\alpha \leq 2$. Taking a different approach, St. Laurent and Garrett (2002) examined the first order correction to linear theory estimates of energy flux for sinusoidal topography of subcritical steepness ($s/\alpha < 1$), finding that $E_f = E_{f(\text{linear})} (1 + \frac{1}{4}(s/\alpha)^2 + \dots)$. Full series expansions for the full corrections for sinusoidal and gaussian topographies were derived by Balmforth et al. (2002) for increasing steepness up to the critical condition ($s/\alpha = 1$). They find increased levels of conversion at critical slopes, though the increase varies from only 14% for the gaussian ridge to 56% for the sinusoidal case.

Models for generation at abrupt depth discontinuities ($s/\alpha = \infty$) have also been formulated. Rattray (1960) considered the first-mode baroclinic response to barotropic flow over shelf topography. Stigebrandt (1980) also considered a topographic step and examined the full spectrum of baroclinic modes. In addition to re-examining internal tides at a step, St. Laurent et al. (2003) consider generation at a knife-edge ridge, a top hat-ridge, and a top-hat trench. They argue that the knife-edge serves as a simple model for calculating internal tide energy flux from tall oceanic ridges.

Here, we present two internal tide energy flux estimates. For the case of internal tide generation at mid-ocean ridge sites, the dominant energy flux is generated by bathymetry that is subcritical ($s/\alpha < 1$). St. Laurent and Garrett (2002) used a linearized model to examine the energy flux spectrum for the semidiurnal internal tide at a Mid-Atlantic Ridge site (Fig. 2a). The energy flux spectrum is clearly ‘‘red,’’ with modes 1-10 accounting for 60% of the total energy flux. This can be contrasted to an estimate for supercritical topography ($s/\alpha > 1$). St. Laurent et al. (2003) considered energy flux generated by tidal flow over a knife-edge ridge (Fig. 2b). In this calculation, the ridge height was taken as 3/4 of the water depth ($\delta = 0.75$), with a deep water barotropic current amplitude of 0.015 m s^{-1} . St. Laurent et al. (2003) argue that the knife-edge is a good model for general tall ridges in the ocean. Here, the knife-edge calculation is compared to an observational based estimate of internal tide energy flux from the Hawaiian Ridge (Fig. 2b). The observationally based estimate was calculated using the measured perturbation pressure and velocity profiles from the 3000-m isobath. These measured properties were projected onto the first fourteen flat-bottom internal wave modes. The same dimension values for buoyancy frequency ($N = 0.004 \text{ s}^{-1}$) and Coriolis frequency ($5.5 \times 10^{-5} \text{ s}^{-1}$) were used for both the knife-edge and observational estimates; wave modes for the knife-edge ridge were calculated for a water depth of 3000 m. As shown in the figure, both the knife-edge and observationally based spectra are red. Furthermore, the spectra show excellent correspondence in modal content. Modes 1-10 account for more than 95% of both the modeled and observed energy flux; in fact, modes 1 and 2 account for 88% of the baroclinic energy flux in both the observationally based and model estimate. The generation of low mode internal tides is clearly favored by both rough mid-ocean ridge topography and abrupt Hawaii-like ridges alike.

The shear (u_z) of the generated internal tides is also of interest, as the Richardson number ($Ri = N^2/u_z^2$) is a crucial stability parameter for baroclinic flow. St. Laurent and Garrett (2002) examined the shear of in-

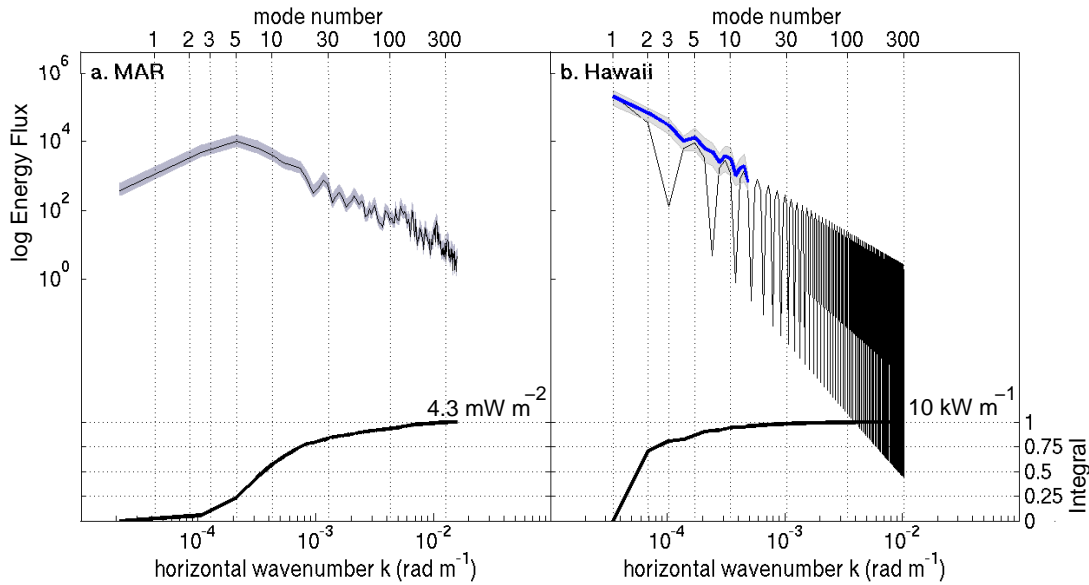


Figure 2. (a) Energy flux spectrum for subcritical internal tide generation at a Mid-Atlantic Ridge site. Multibeam bathymetry data were used to calculate the spectrum, and the standard error confidence band is shown. The spectrum has units of $(\text{mW m}^{-2})/(\text{rad m}^{-1})$, and the net integrated energy flux is 4.3 mW m^{-2} . (b) Energy flux for supercritical internal tide generation at a knife-edge ridge, assumed to be a simple representation of the energy flux spectrum from the Hawaiian Ridge. The spectrum has units of $(\text{kW m}^{-1})/(\text{rad m}^{-1})$, and the net integrated energy flux is 10 kW m^{-2} . In both panels, the normalized cumulative integral of energy flux is shown. In b, an observationally based estimate of the energy flux spectrum at the 3000-m isobath of the Hawaiian Ridge is shown (confidence band in blue shading).

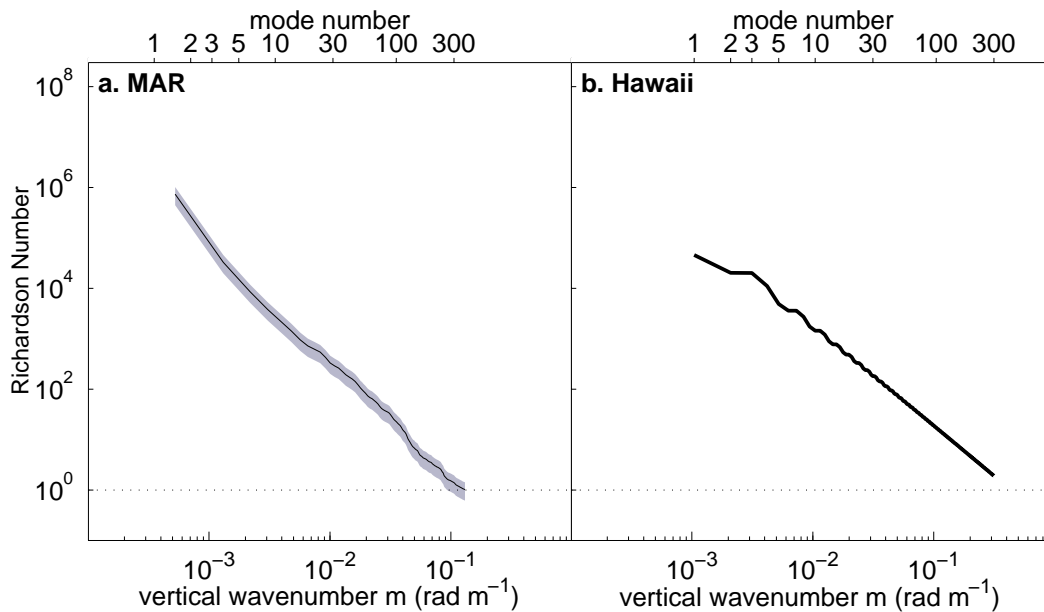


Figure 3. The Richardson number estimated by integrating the cumulative shear variance of increasing modes for internal tides generated at (a) a mid-ocean ridge and (b) a knife-edge ridge. In both panels, the first 300 baroclinic modes are shown. A Richardson number of unity is indicated for reference.

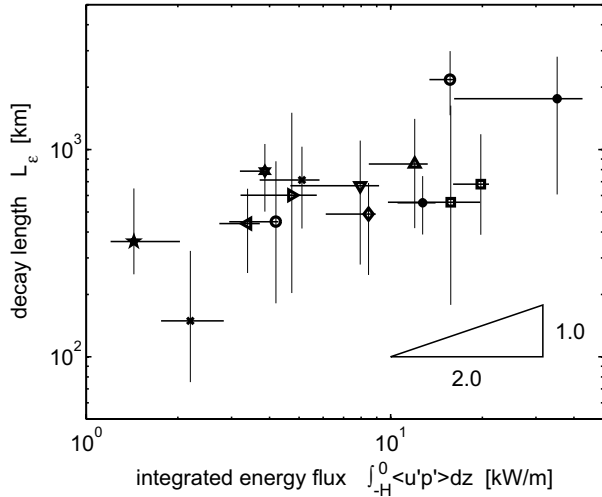


Figure 4. Spatial decay scale as a function of depth-integrated energy flux, as estimated from observations along the 3000-m isobath at the Hawaiian Ridge. Symbols represent averages from 16 different station occupations; error bars represent 95% bootstrap confidence intervals (based on computations from a subset of data from each station occupation).

ternal tides generated at mid-ocean ridge topography. They computed the cumulative integral of shear variance as a function of vertical wavenumber ($u_z^2(m)$), and then defined $Ri(m) = N^2/u_z^2(m)$. They found that, in the absence of background sheared currents, the Richardson number is large for the wavelengths that dominate the energy flux (Fig. 3a). *St. Laurent and Garrett* (2002) therefore conclude that shear instability is not a primary influence on the low mode energy flux generated at subcritical topography. The Richardson number for the knife-edge ridge discussed above is considered here (Fig. 3b). As is the case for the mid-ocean ridge site, the first 300 modes of the knife-edge are characterized by $Ri > 1$. We note that in both cases, the Richardson numbers clearly drops below unity when very high modes are accounted for in the shear variance. In fact, for the case of supercritical wave generation, inviscid theories, like that of *St. Laurent et al.* (2003) for knife-edge generation, give infinite integrated shear variance. These extremely high modes manifest their shear in a narrow beam, as are observed at supercritical generation sites. As shown by *Lien and Gregg* (2001), large amounts of dissipation can occur along the path of the beam. However, it seems unlikely that the energy flux carried by the lowest modes is influenced by the low Richardson numbers associated with beam-like structures.

3. Internal tide radiation and decay

Given the dominance of low mode generation, much of the internal tide’s energy flux will radiate away from the generation region. Direct evidence for radiated low modes has been documented at a number of internal tide generations sites. *Ray and Mitchum* (1996) have examined the sea-surface elevation signature of low mode semidiurnal tides generated at Hawaii. They find that a coherent signal of radiation extending over 1000 km to the north and south of the ridge. *Ray and Mitchum* (1997) estimate that the mode-1 radiation from Hawaii accounts for 15 GW of energy flux. This compares to 20 GW as estimated by *Egbert and Ray* (2000) for the total barotropic tidal power loss at Hawaii. In an approach similar to Ray and Mitchum, *Cummins et al.* (2001) have examined low mode internal tides radiating from the Aleutian Ridge. They also find a coherent signal of radiation extending 1000 km from the ridge. There, the total radiated energy flux away from the ridge is estimated at 2 GW. A recent examination of current meter data from a number of deep ocean sites (*Alford*, 2003b) confirms that the radiated internal tides are directed away from topographic source regions. *Alford* (2003b) finds that baroclinic currents of tidal frequency are a significant signal in measured records far from sites of generation.

Simultaneous observations of fine- and microstructure made during HOME permit estimation of a spatial decay scale for the radiated tides. Measurements of the baroclinic velocity and pressure were used to calculate the baroclinic energy flux ($\langle v'p' \rangle$) following the method of *Kunze et al.* (2002a). The depth-integrated energy flux was compared to the depth-integrated turbulent energy dissipation (ϵ) at each of 16 stations located on both the north and south flanks of the 3000-m isobath. These permit calculation of a decay length of the radiated tide:

$$L_\epsilon \simeq \frac{\int \langle v'p' \rangle dz}{\int \rho \epsilon dz}, \quad (3)$$

as shown in Figure 4. In (3), the vertical integrals were computed over the depth range between 100 m and the bottom (i.e., neglecting the surface-influenced 100 m). This decay scale represents the e-folding scale for an internal wave assuming the dissipation rate is constant (and equal to that of the 3000-m isobath) along the path of propagation if radial dispersion is neglected. Since the actual dissipation rate is observed to decay with distance from the Hawaiian Ridge (*Klymak et al.*, 2002), L_ϵ is likely an underestimate of the real e-folding scale. The O(1000) km decay scales are consistent with the correlation scales documented by *Ray and Mitchum* (1996) for the lowest mode internal tide.

Figure 4 shows that the largest decay scales are as-

sociated with the largest energy fluxes. In other words, the integrated dissipation is fractionally less important at sites of strong energy flux. We postulate the presence of dissipative high modes is only weakly related to the amount of low mode energy flux generation, so that dissipation occurs in higher proportion at sites of weak generation.

In the following we consider the processes that influence the evolution of the radiated internal tide spectrum and contribute to its decay. These include wave-wave interactions and bottom scattering. The efficiency of these processes will determine whether the internal tide dissipates near the generation region, or far away.

a. Wave-wave interactions

The transfer of energy between wave modes due to wave-wave interactions has been the focus of a number of studies, and a review of this subject was given by Müller *et al.* (1986). *Olbers and Pomphrey* (1981) and *Hirst* (1991, 1996) specifically examined the wave-wave interactions between the internal tide and the internal-wave continuum, and estimated the time scale for the energy transfer away from modes 1-10 to higher modes. They considered the Parametric Subharmonic Instability (PSI) resonant interaction, which transfers tidal energy with frequency ω to higher vertical wavenumbers with frequency $\omega/2$. Thus, the PSI mechanism is an effective mechanism for dissipating the M_2 internal tides at latitudes less than about 30° . Estimates of the dissipation time scale for the M_2 internal tides by PSI are given in Figure 5 (adapted from *Olbers*, 1983). The transfer time scale is $O(100)$ days for mode 1, consistent with the observed weak spatial decay of low mode internal tides generated at the Hawaiian Ridge (*Ray and Mitchum*, 1996) and the Aleutian Ridge (*Cummins et al.*, 2001). The PSI transfer time scale decreases to $O(1)$ day for mode 10. *Hirst* (1996) discusses conditions where strong tidal forcing can result in reduced transfer time scales, even for low mode internal tides.

Other studies have considered the additional resonant interactions occurring in the general internal wave continuum over the range of frequencies between f and N . The “elastic scattering” and “induced diffusion” interactions may influence internal tides at all latitudes. In all cases, wave interaction time scales for low modes with tidal frequencies typically exceed $O(10)$ days (*Müller et al.*, 1986; *Hirst*, 1991).

It is useful to compare the wave interaction time scale to the time for a wave group to travel from bottom to surface and back again, defined according to $\tau_g = 2 \int c_g^{-1} dz$, where the integral is over the ocean depth and c_g is the vertical component of the group speed. The latitude and mode number dependent

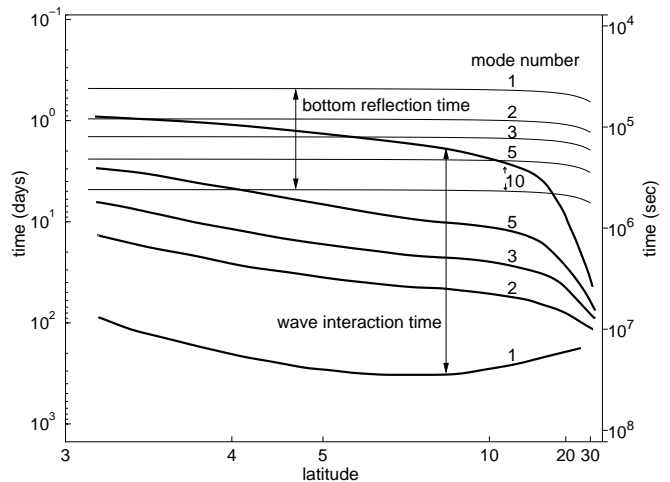


Figure 5. The time scales for wave-wave (PSI) interactions between the M_2 internal tide and the internal wave continuum for modes 1, 2, 3, 5, and 10, adapted from *Olbers* (1983). The Parametric Subharmonic Instability interaction for the M_2 tide occurs equatorward of $\pm 30^\circ$ latitude. Bottom reflection times for the various modes were estimated for an exponential stratification over a depth of 4000 m.

curves for τ_g were computed using $N = N_0 e^{z/b}$ with $(b, N_0) = (1300 \text{ m}, 0.005 \text{ s}^{-1})$, and the results are shown in Figure 5. Low modes have the fastest group speeds, with $\tau_g \leq 12$ hrs for mode 1 and $\tau_g \geq 4$ days for mode 10. Thus, low modes will easily complete one round trip between the bottom and surface before experiencing the effects of wave-wave interactions. For modes $j \geq 10$, energy transfer to higher modes will occur over a time scale comparable to, or faster than, the bottom reflection time. Thus, wave-wave interactions may be the dominant mechanism of spectral evolution for high mode components of the internal tide, while bottom reflection may be significant for low modes.

b. Bottom reflection and topographic scattering

The interaction of internal waves with bottom bathymetry is often discussed in terms of wave reflection from sloping topography and wave scattering from rough topography. Particular attention has been given to reflection from planar slopes (e.g., *Eriksen*, 1982). Reflection from slopes with nonplanar geometries has been considered by *Gilbert and Garrett* (1989) and *Müller and Liu* (2000a,b). Scattering of waves from random rough topography was considered by *Müller and Xu* (1992), while *Thorpe* (2001) considered scattering from rough topography with an underlying slope. The latter

studies are relevant to our discussion of low mode internal tides from arbitrary topography in the deep ocean.

As discussed by *Müller and Xu* (1992), both reflection and scattering redistribute the energy flux in wavenumber space. Müller and Xu (1992) find that scattering is more efficient than reflection at redistributing energy flux to higher modes, particularly at tidal and near inertial frequencies. However, *Müller and Xu* (1992) find less than 10% of the incoming radiation is redistributed during a scattering event at typical deep ocean topography. Most of the incoming radiation undergoes pure reflection as from a flat bottom, such that the wavenumber content of the spectrum is mostly preserved. *St. Laurent and Garrett* (2002) examined the scattering of the mode-1 internal tide through a “second generation” calculation. They find mode-1 scattering occurs with an efficiency of about 10%, comparable to the efficiencies estimated by *Müller and Xu* (1992).

4. Dissipation at generation sites

Sites of strong internal tide generation can both radiate low mode internal waves that propagate O(1000) km distances before dissipating and generate high-wavenumber motions which dissipate locally. Here we attempt to assess the fraction of internal tide energy flux that dissipates as turbulence near generation regions. We define the “local dissipation fraction” as,

$$q = \frac{\langle \int \rho \epsilon dz \rangle}{E_f}, \quad (4)$$

where the column integrated dissipation in (4) is space/time averaged, and E_f is the average energy flux per unit area.

Direct measurements of turbulent dissipation rates above Mid-Atlantic Ridge topography have been described by *St. Laurent et al.* (2001). These data were collected over two 4-week sample periods in a region between 12° – 22°W longitude and 20° – 25°S latitude above fracture zone topography in the Brazil Basin. The average dissipation rate, vertically integrated to a height of 2000 m above the bottom, was 1.2 ± 0.2 mW m⁻². If this dissipated energy is assumed to be provided by the internal tide, it can be compared to estimates of generated internal tide energy flux. *St. Laurent and Garrett* (2002) considered the internal tide energy flux over the region between 8° – 20°W longitude and 22° – 32°S latitude, and found 4 ± 1 mW m⁻² as the spatially averaged generated power. Taken together, these dissipation and generation estimates suggest an average local dissipation fraction of $q = 0.3 \pm 0.1$.

Comparison of the estimates of *Ray and Mitchum* (1997) and *Egbert and Ray* (2000) for internal tides at

the the Hawaiian Ridge can also be used to estimate the local dissipation fraction. These estimates imply that at least 75% of the generated energy flux is radiated to the far field in mode 1, leaving $q \leq 0.25$ as the fraction that dissipates near the ridge. Two considerations make this preliminary estimate uncertain. First, *Ray and Mitchum*’s 15 GW only accounts for the energy flux in the lowest mode. Direct observations (Figure 2b and *Kunze et al.*, 2002b), indicate that modes 2 and higher carry an appreciable fraction of the energy flux. Second, some of the 20 GW of barotropic power loss at Hawaii may be dissipated by frictional drag along the shallow areas of the ridge. Further analysis of HOME observations will establish a more certain estimate.

Althaus et al. (2003) have also estimated the local dissipation fraction using their measurements of finestructure and microstructure from the Mendocino Escarpment site. They used the method of *Kunze et al.* (2002a) to estimate the baroclinic energy flux $\langle v'p' \rangle$ of radiated internal tides. It is possible to rewrite (4) as

$$q = \frac{\langle \int \rho \epsilon dz \rangle}{\nabla \cdot \langle \int v'p' dz \rangle + \langle \int \rho \epsilon dz \rangle}. \quad (5)$$

Althaus et al. (2003) report that $q \simeq 0.01$ for the local dissipation fraction along the ridge crest of Mendocino Escarpment. Dissipation occurring at sites where the ridge-generated beam refracts from the sea surface is not included in this estimate.

It is clear that the local dissipation fraction may have an order-of-magnitude variability ($q \sim 0.01$ – 0.3). This likely depends on the details of the generating topography (e.g., $\delta, s/\alpha, kU_0/\omega$), and a multitude of other factors.

5. Parameterizing local mixing

St. Laurent et al. (2002) have suggested a semi-empirical operational scheme for estimating enhanced turbulent mixing rates in regions where internal tides are generated. They build on a parameterization of internal tide energy flux used with a hydrodynamic model for the tides (*Jayne and St. Laurent*, 2001). *Jayne and St. Laurent* (2001) estimated the energy flux as

$$E_f \simeq \frac{1}{2} \rho N_b \kappa h^2 U^2. \quad (6)$$

Here ρ is the reference density of seawater, N_b is the buoyancy frequency along the seafloor, and (κ, h) are the wavenumber and amplitude scales for the topographic roughness. The barotropic tidal speed U is determined through solution of the Laplace tidal equations. Further details of the barotropic model and the tidal simulation are given by *Jayne and St. Laurent*

(2001). They find that estimates from (6) account for about 1 TW of energy flux into the deep ocean. This provides a constraint on the amount of energy available for the enhancement of turbulence near sites of internal tide generation. However, as we have discussed, not all of the generated energy flux contributes to local mixing, since some energy radiates away from the generation sites as low mode waves. Only $q \cdot E_f$ is dissipated locally.

Motivated by the dissipation and generation estimates from the abyssal Brazil Basin, we propose an initial estimate of the local dissipation fraction of $q = 0.3 \pm 0.1$. We have limited information on which to assess the variability of this parameter for different internal tide generation regions, though we suspect it to depend on the “color” of the generated energy flux spectrum. While we expect $q \simeq 0.3$ to be appropriate for the mid-ocean ridge regions similar to the Brazil Basin, it may be an overestimate for regions like the Mendocino Escarpment (*Althaus et al.*, 2003) or the Hawaiian Ridge.

Our model for the turbulent dissipation rate follows as

$$\epsilon \simeq (q/\rho)E_f(x, y)F(z), \quad (7)$$

where $E_f(x, y)$ is the time-averaged map of generated internal tide energy flux, and $F(z)$ is a function for the vertical structure of the dissipation, chosen to satisfy energy conservation within an integrated vertical column, $\int_{-H}^0 F(z)dz = 1$. The parameterization for the turbulent diffusivity follows from the *Osborn* (1980) relation for the mechanical energy budget of turbulence,

$$k_v \simeq \frac{\Gamma q E_f(x, y) F(z)}{\rho N^2}. \quad (8)$$

Here, Γ is related to the mixing efficiency of turbulence, and $\Gamma = 0.2$ is generally used (*Osborn*, 1980). The diffusivity given in (8) is meant to quantify only the enhanced levels of mixing supported by the topographically enhanced dissipation of internal tide energy. A background diffusivity of $0.1 \times 10^{-4} \text{ m}^2 \text{ s}^{-1}$ is still assumed to be sustained in all regions, and must be added to the estimate from (8). Contributions to the diffusivity from other sources of enhanced mixing, such as turbulence in critical layers and frictional boundary layers, could also be added to (8).

In the estimates we present here, our selection of the vertical structure function $F(z)$ in (7) and (8) is motivated by turbulence observations shown in Figure 1. These observations suggest that the dissipation rate has a similar structure at many sites, and can roughly be modeled as an exponential function that decays away from the topography. Specifically, we use a dissipation profile of the form $\epsilon(z) = \epsilon_0 \exp(-(H+z)/\zeta)$, where

ζ is the vertical decay scale, and ϵ_0 is the maximum dissipation rate at the bottom, $z = -H$. This gives

$$F(z) = \frac{e^{-(H+z)/\zeta}}{\zeta(1 - e^{-H/\zeta})}. \quad (9)$$

St. Laurent et al. (2002) examined a number of diffusivity sections estimated using (8) and (9) with $\zeta = 500 \text{ m}$. We note that this choice is consistent with profiles of ϵ shown in Figure 1, but is otherwise somewhat arbitrary. Stratification estimates were derived from *Levitus and Boyer* (1994) and *Levitus et al.* (1994). These reveal significant spatial variations in tidal mixing, especially with respect to spatial variations in bottom roughness.

As an example, a zonal section of diffusivity, averaged in the latitude band between 24°S and 28°S , is shown in Figure 6 for the South Atlantic. The Mid-Atlantic Ridge (15°W), and the Walvis Ridge (5°E) are sites where elevated levels of diffusivity reach the upper ocean. At abyssal depths, diffusivity estimates in the Angola Basin exceed those in the Brazil Basin. This signal is tied to differences in abyssal stratification, with weaker stratification occurring in the Angola Basin. Since the internal tide energy flux is proportional to N_b , the diffusivity scales as N_b^{-1} at these abyssal depths. In Figure 6, it appears that most enhanced levels of mixing occur within the envelope (the min/max range in local bathymetry) of rough topography characterizing the section. Moreover, the vertical extent of strongest enhancement generally does not fill the vertical extent of the topography envelope. This is consistent with observations of turbulence above rough topography (e.g., Figure 2 of *St. Laurent et al.*, 2001). Our section of diffusivity across the Brazil Basin (Fig. 6) may be compared to the section of *Polzin et al.* (1997), with notice to the significant differences in color axes used in both presentations. In addition, *Polzin et al.* (1997) collapsed two survey transects into one zonal section and show bathymetry from only one transect; enhanced diffusivity appearing at significant heights above this bathymetry may therefore occur much closer to the bottom.

This mixing scheme is a preliminary attempt to formulate internal tide dissipation in terms of the topographically generated internal tide. It simply assumes that the internal tide energy flux is generated according to (6) and that a fraction ($q = 0.3$) of the energy flux is dissipated locally. A more physically based representation would predict values of q and ζ that vary spatially and depend on the details of the bathymetry and the tidal forcing. At this point, however, it is difficult to accurately evaluate the value of q even in a region where substantial fine- and microstructure ob-

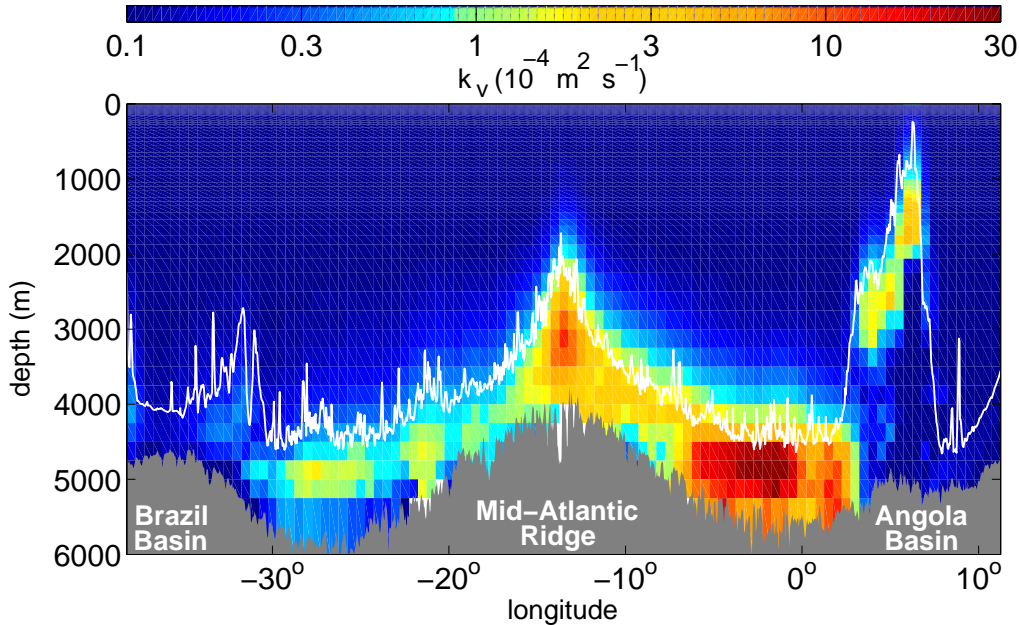


Figure 6. Estimated diffusivity section for the latitude band between $24^\circ - 28^\circ\text{S}$ for the Atlantic. A background diffusivity of $0.1 \times 10^{-4} \text{ m}^2 \text{ s}^{-1}$ has been added to the parameterized estimates from (8). The envelope defined by deepest (shaded) and shallowest (white line) bathymetry in the 4° latitude band is indicated.

servations have been made, so it makes little sense to introduce additional *tunable parameters* into this simple parameterization.

This approach is meant to be a first-round effort to model enhanced mixing rates in regions of internal tide generation. It is intended for application in OGCMs, particularly those used at coarse resolution to study the long time scales associated with the thermohaline circulation. A preliminary implementation of the parameterization in such a model is discussed by *Simmons et al.* (2002), whose initial results suggest that the equilibrium behavior of OGCM simulation is significantly improved by this new mixing scheme. Thus, it is hoped that the current parameterization, though crude, may serve as a useful tool in studies of long term climate.

6. Discussion

Having considered the various mechanisms that can act to degrade internal tides into turbulence, it is possible to speculate about the nature of internal tide driven mixing in the deep ocean. Low mode waves are relatively uninfluenced by wave-wave interactions and their Richardson numbers are large. In regions where additional sheared currents are absent, low modes will propagate away from their generation sites, carrying much of the generated energy flux. The lateral distance for one round trip between the bottom and surface can be

estimated using the characteristic equation for a tidal beam, $dx/dz = \alpha^{-1}$, such that

$$\Delta x = 2 \int_{-H}^0 \left(\frac{N^2(z) - \omega^2}{\omega^2 - f^2} \right)^{1/2} dz. \quad (10)$$

For typical stratification in the deep ocean, this radiation distance is $\Delta x \simeq 100$ km. Thus, waves corresponding to low modes can be expected to travel $O(100)$ km before scattering from topography. During topographic scattering, much of the low mode energy flux is preserved, suggesting that low modes can radiate through many bottom encounters. Observations of internal tides generated at Hawaii (*Ray and Mitchum, 1996*) and the Aleutian Ridge (*Cummins et al., 2001*) demonstrate that low modes can be tracked for $O(1000)$ km away from their generation site.

Mixing driven by the internal tide must be supported by a wavefield with sufficient amplitude and high-wavenumber content such that the superposition of waves is susceptible to shear- or convective-instability. At sites where critical generation occurs, elevated levels of shear along radiated beams will support enhanced turbulence. Additionally, the transfer of low mode energy to smaller scales will be enhanced in regions of rough or near-critical topography where wave reflection and scattering occur. Wave-wave interactions act efficiently on higher wavenumbers, providing another mechanism for converting internal tides into turbulence.

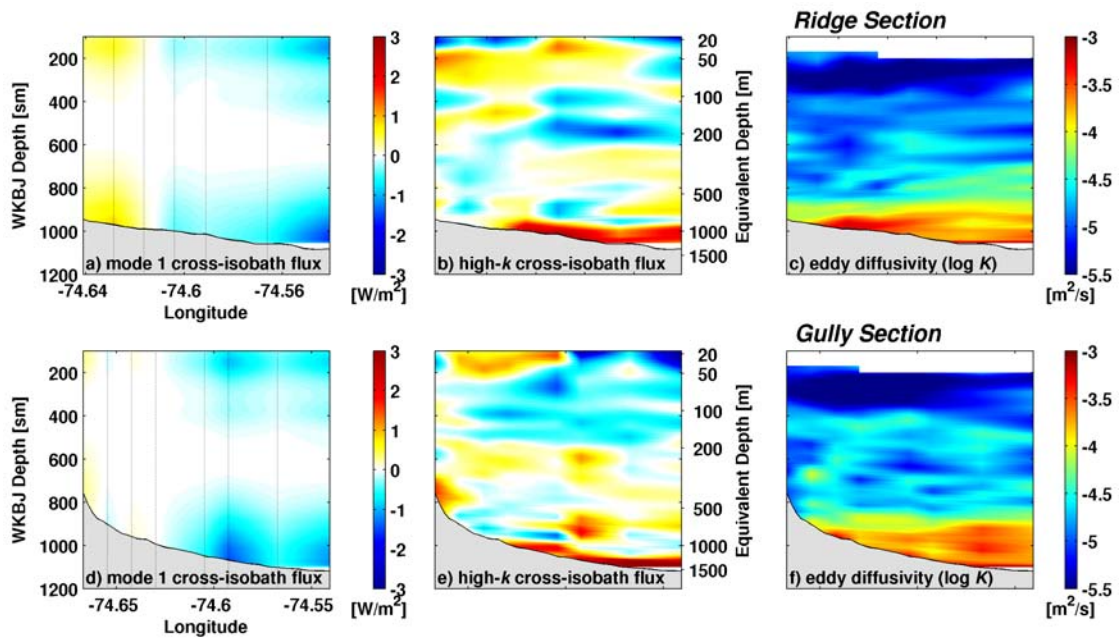


Figure 7. Spatial distribution of cross-isobath energy flux and inferred eddy diffusivity along a ridge top (top row) and through its neighboring gully (bottom row) over the continental slope of the Mid-Atlantic Bight. The energy flux computed from projections onto the mode-1 structure functions is shown in a and d; the high wavenumbers (total flux minus mode 1) are shown in b and e. The eddy diffusivity inferred from the Gregg-Henyey scaling applied to the finescale shear (c and f) is intensified near the bottom below 1000 m, approaching $10 \times 10^{-4} \text{ m}^2 \text{ s}^{-1}$. The low mode convergence exceeds the high-wavenumber divergence; the excess is more than sufficient to supply the observed dissipation.

The Parametric Subharmonic Instability interaction is particularly effective, since it specifically moves energy to higher modes. However, the PSI mechanism for tidal frequencies is only effective at low latitudes. The effectiveness of other classes of wave-wave interactions at transferring wave energy to higher modes is unclear, though some ideas are presented by *Polzin (1999)*. Numerical studies such as those by *MacKinnon and Winters (2003 – this volume)* will further elucidate the mechanisms of this wave-to-turbulence energy transfer.

The wave-wave interaction time scale for mode 10 is roughly equal to the time scale over which the mode 10 tidal beam completes a round trip between the bottom and surface. Over this characteristic time scale, the mode 10 tidal beam radiates roughly 100 km from the generation site. Higher modes will be increasingly influenced by the wave-wave interactions over shorter time and distance scales. We suggest that for a given internal tide generation event, waves with mode number less than 10 are likely to radiate away, while those greater than 10 dissipate locally. For the MAR site discussed in Section 2, this suggests that roughly 1/3 of the generated power, about $1\text{--}2 \text{ mW m}^{-2}$, may dissipate as turbulence at this site. For our knife-edge model of the Hawaiian Ridge, modes greater than 10 represent only 5% of the generated power. At other sites, the amount of energy flux available in modes greater than 10 will clearly depend on the details of the energy spectrum and on the amplitude of the tidal forcing.

Low modes that radiate away will be influenced by topographic scattering. Energy scattered to higher modes is more likely to dissipate, so topographic scattering provides a mechanism for driving mixing away from an internal tide generation site. However, the efficiency of topographic scattering is low, with only a small fraction of low mode energy flux being transferred to higher modes during each scattering event. It is possible that while the scattering efficiency for general topographies is low, certain topographic sites may favor enhanced scattering. For example, *Gilbert and Garrett (1989)* and *Müller and Liu (2000b)* find convex topographies are more efficient than linear or concave topographies at scattering energy to high modes. Thus, in addition to the internal tides generated at such sites, convex topographies may be favored sites for the dissipation of incoming internal tide energy. At such sites, the scattered waves could act as a catalyst for dissipating the locally generated waves, since elevated shear levels in the scattered waves will contribute to a lower overall Richardson number.

Given the inefficient nature of topographic scattering at general topographies, it is likely that low mode internal tides radiate much of their energy through multi-

ple bottom reflections over $O(1000)$ km distances. Low modes must dissipate somewhere, but the nature of low mode dissipation is particularly unclear. Perhaps low modes are preferentially dissipated in regions of enhanced sheared currents, such as the equatorial undercurrents. Perhaps low modes propagate onto the continental shelves, where they produce bores and solibores, or simply dissipate in shallow waters. *Nash et al. (2003)* present observations from the continental slope of the U.S. Mid-Atlantic Bight (Fig. 7). They suggest the incoming low mode internal tide is reflected and scattered into high wavenumbers as it encounters the near-critical Virginia Slope. The resultant high wavenumbers presumably decay locally to produce the observed elevated dissipation and mixing rates. *Nash et al. (2003)* suggest that many continental slopes are near-critical with respect to a semidiurnal characteristic. Furthermore, it may be possible to model the elevated dissipation in these regions using a model for wave scattering from large scale bathymetry data (*Smith and Sandwell, 1997*), provided that the incoming low mode energy flux is known. Improved global estimates of the long-range propagation of the internal tide (i.e., *Alford 2003b*) may help to quantify these low mode waves and their eventual fate.

Finally, perhaps low modes are dissipated throughout the interior of the deep ocean, under the slow evolution of wave-wave interactions. In this scenario, much of the energy in low mode internal tides would be uniformly dispersed through the oceanic interior. The dissipation of this energy would contribute to background levels of turbulence everywhere. The fate of low mode internal tides, however, remains as a primary question.

Acknowledgments. Data presented in this report were collected by a number of investigators. We thank Tom Sanford, Eric Kunze and Craig Lee for their efforts in the collection and interpretation of Hawaii Ocean Mixing Experiment data presented in this report. Additionally, we are grateful for Figure 1 data contributed by Jim Moum and Kurt Polzin. This research has been funded by grants from NSF and ONR.

References

- Alford, M. H., Internal swell generation: The spatial distribution of energy flux from the wind to mixed-layer near-inertial motions, *J. Phys. Oceanogr.* 31, 2359–2386, 2001.
- Alford, M. H., Improved global maps and 54-year history of wind-work on ocean inertial motions, *Geophys. Res. Lett.*, 30, 10.1029/2002GL016614, 2003a.
- Alford, M. H., Redistribution of energy available for ocean mixing by long-range propagation of internal waves, *Nature*, 423, 159–162, 2003b.

- Althaus, A.M., E. Kunze, and T. B. Sanford, Internal tide radiation from Mendocino Escarpment, *J. Phys. Oceanogr.*, 33, 1510–1527, 2003.
- Baines, P. G., The generation of internal tides by flat-bump topography, *Deep-Sea Res.*, 20, 179–205, 1973.
- Baines, P. G., On internal tide generation models, *Deep-Sea Res.*, 29, 307–338, 1982.
- Balmforth, N. J., G. R. Ierley, and W. R. Young, Tidal conversion by subcritical topography, *J. Phys. Oceanogr.*, 32, 2900–2914, 2002.
- Bell, T. H., Lee waves in stratified flows with simple harmonic time dependence, *J. Fluid Mech.*, 67, 705–722, 1975.
- Cox, C. S., and H. Sandstrom, Coupling of surface and internal waves in water of variable depth, *Journal of the Oceanographic Society of Japan*, 20th Anniversary Volume, 499–513, 1962.
- Craig, P. D., Solutions for internal tide generation over coastal topography. *J. Mar. Res.*, 45, 83–105, 1987.
- Cummins, P. F., J. Y. Cherniawski, and M. G. G. Foreman, North Pacific internal tides from the Aleutian Ridge: Altimeter observations and modelling, *J. Mar. Res.*, 59, 167–191, 2001.
- Egbert, G. D., Tidal data inversion: Interpolation and inference, *Progress in Oceanography*, 40, 81–108, 1997.
- Egbert, G. D., A. F. Bennett, and M. G. G. Foreman, TOPEX/POSEIDON tides estimated using a global inverse model, *J. Geophys. Res.*, 99, 24821–24852, 1994.
- Egbert, G. D., and R. D. Ray, Significant dissipation of tidal energy in the deep ocean inferred from satellite altimeter data. *Nature*, 405, 775–778, 2000.
- Egbert, G. D., and R. D. Ray, Estimates of M2 tidal energy dissipation from TOPEX/POSEIDON altimeter data, *J. Geophys. Res.*, 106, 22475–22502, 2001.
- Eriksen, C., Observations of internal wave reflection off sloping bottoms, *J. Geophys. Res.*, 87, 525–538, 1982.
- Gilbert, D., and C. Garrett, Implications for ocean mixing of internal waves scattering off irregular topography, *J. Phys. Oceanogr.*, 19, 1716–1729, 1989.
- Hendershott, M. C., Long waves and ocean tides. *Evolution of Physical Oceanography*, B. A. Warren and C. Wunsch, Eds., The MIT Press, 292–341, 1981.
- Hibiya, T., Generation mechanism of of internal waves by tidal flow over a sill, *J. Geophys. Res.*, 91, 7696–7708, 1986.
- Hirst, E., Internal wave-wave resonance theory: Fundamentals and limitations, *Dynamics of Oceanic Internal Gravity Waves*, Proc. ‘Aha Huliko’a Hawaiian Winter Workshop, P. Müller and D. Henderson, Eds., SOEST, 211–226, 1991.
- Hirst, E., *Resonant Instability of Internal Tides*, Ph. D. dissertation, University of Washington, 92 pp, 1996.
- Jayne, S. R., and L. C. St. Laurent, Parameterizing tidal dissipation over rough topography, *Geophys. Res. Lett.*, 28, 811–814, 2001.
- Khatiwala, S., Generation of internal tides in an ocean of finite depth: analytical and numerical calculations, *Deep-Sea Res.*, 50, 3–21, 2003.
- Klymak, J. M., J. N. Moum, and A. Perlin, Observations of boundary mixing in the Hawaiian Ridge system, *EOS, Trans. AGU*, 83(4), Ocean Sciences Meet. Suppl., Abstract OS41E-77, 2002.
- Kunze, E., and J. M. Toole, Tidally driven vorticity, diurnal shear, and turbulence atop Fieberling Seamount, *J. Phys. Oceanogr.*, 27, 2663–2693, 1997.
- Kunze, E., L. K. Rosenfeld, G. S. Carter, and M. C. Gregg, Internal waves in the Monterey submarine canyon, *J. Phys. Oceanogr.*, 32, 1890–1913, 2002a.
- Kunze, E., T. B. Sanford, C. M. Lee, and J. D. Nash, Internal tide radiation and turbulence and turbulence along the Hawaiian Ridge, *EOS, Trans. AGU*, 83(4), Ocean Sciences Meet. Suppl., Abstract OS32P-01, 2002b.
- Li, M., Energetics of internal tides radiated from deep-ocean topographic features, *J. Phys. Oceanogr.*, submitted, 2003.
- Ledwell, J. R., E. T. Montgomery, K. L. Polzin, L. C. St. Laurent, R. W. Schmitt, and J. M. Toole, Mixing over rough topography in the Brazil Basin, *Nature*, 403, 179–182, 2000.
- Levitus, S., R. Burgett, and T. P. Boyer, *World Ocean Atlas 1994, Volume 3: Salinity*, NOAA Atlas NESDIS 3, U.S. Department of Commerce, Washington, D.C., 1994.
- Levitus, S., and T. P. Boyer, *World Ocean Atlas 1994, Volume 4: Temperature*, NOAA Atlas NESDIS 4, U.S. Department of Commerce, Washington, D.C., 1994.
- Lien, R.-C., and M. C. Gregg, Observations of turbulence in a tidal beam and across a coastal ridge, *J. Geophys. Res.*, 106, 4575–4592, 2001.
- Llewellyn Smith, S. G., and W. R. Young, Conversion of the barotropic tide, *J. Phys. Oceanogr.*, 32, 1554–1566, 2001.
- Lueck, R. G., and T. D. Mudge, Topographically induced mixing around a shallow seamount, *Science*, 276, 1831–1833, 1997.
- Moum, J. N., D. R. Caldwell, J. D. Nash, and G. D. Gunderson, Observations of boundary mixing over the continental slope, *J. Phys. Oceanogr.*, 32, 2113–2130, 2002.
- Müller, P., G. Holloway, F. Henyey, and N. Pomphrey, Non-linear interactions among internal gravity waves, *Rev. Geophys.*, 24, 493–536, 1986.
- Müller, P., and N. Xu, Scattering of oceanic internal waves off random bottom topography, *J. Phys. Oceanogr.*, 22, 474–488, 1992.
- Müller, P., and X. Liu, Scattering of internal waves at finite topography in two dimensions. Part I: Theory and case studies, *J. Phys. Oceanogr.*, 30, 532–549, 2000a.
- Müller, P., and X. Liu, Scattering of internal waves at finite topography in two dimensions. Part II: Spectral calculations and boundary mixing, *J. Phys. Oceanogr.*, 30, 550–563, 2000b.
- Munk, W., and C. Wunsch, Abyssal recipes II: energetics of tidal and wind mixing, *Deep-Sea Res.*, 45, 1977–2010, 1998.
- Nash, J.D., E. Kunze, J. M. Toole and R. W. Schmitt, Internal tide reflection and turbulent mixing on the continental slope, *J. Phys. Oceanogr.*, submitted, 2003.
- Olbers, D. J., Models of the oceanic internal wave field, *Rev. Geophys.*, 21, 1567–1606, 1983.
- Olbers, D. J., and N. Pomphrey, Disqualifying two candidates for the energy balance of oceanic internal waves, *J. Phys. Oceanogr.*, 11, 1423–1425, 1981.

- Osborn, T. R., Estimates of the local rate of vertical diffusion from dissipation measurements, *J. Phys. Oceanogr.*, 10, 83–89, 1980.
- Pinkel, R., W. Munk, P. Worcester, and others, Ocean mixing studied near Hawaiian Ridge, *EOS Trans. AGU*, 81, pp 545,553, 2000.
- Polzin, K. L., A rough recipe for the energy balance of quasi-steady internal lee waves, *Dynamics of Oceanic Internal Gravity Waves II, Proc. ‘Aha Huliko’a Hawaiian Winter Workshop*, P. Müller and D. Henderson, Eds., Honolulu, HI, University of Hawaii at Manoa, 117–128, 1999.
- Polzin, K. L., J. M. Toole, J. R. Ledwell and R. W. Schmitt, Spatial variability of turbulent mixing in the abyssal ocean, *Science*, 276, 93–96, 1997.
- Rattray, M., On the coastal generation of internal tides, *Tellus*, 12, 54–61, 1960.
- Ray, R., and G. T. Mitchum, Surface manifestation of internal tides generated near Hawaii, *Geophys. Res. Lett.*, 23, 2101–2104, 1996.
- Ray, R., and G. T. Mitchum, Surface manifestation of internal tides in the deep ocean: observations from altimetry and island gauges, *Progress in Oceanography*, 40, 135–162, 1997.
- St. Laurent, L. C., J. M. Toole, and R. W. Schmitt, Buoyancy forcing by turbulence above rough topography in the abyssal Brazil Basin, *J. Phys. Oceanogr.*, 31, 3476–3495, 2001.
- St. Laurent, L. C., and C. Garrett, The role of internal tides in mixing the deep ocean, *J. Phys. Oceanogr.*, 32, 2882–2899, 2002.
- St. Laurent, L. C., H. L. Simmons, and S. R. Jayne, Estimating tidally driven mixing in the deep ocean, *Geophys. Res. Lett.*, 29, 2106, doi:10.1029/2002GL015633, 2002.
- St. Laurent, L., S. Stringer, C. Garrett, and D. Perrault-Joncas, The generation of internal tides at abrupt topography, *Deep-Sea Res., Pt I*, doi:10.1016/S0967-0637(03)00096-7, 2003.
- Simmons, H. L., S. R. Jayne, L. C. St. Laurent, and A. J. Weaver, Tidally driven mixing in a numerical model of the ocean general circulation, *Ocean Modelling*, doi:10.1016/S1463-5003(03)00011-8, 2003.
- Smith, W. H. F., and D. T. Sandwell, Global sea floor topography from satellite altimetry and ship depth soundings, *Science*, 277, 1956–1962, 1997.
- Seibold, E., and W. H. Berger, *The Sea Floor - An Introduction to Marine Geology*, Springer-Verlag, 356pp, 1996.
- Stigebrandt, A., Some aspects of tidal interaction with Fjord Constrictions, *Estuarine and Coastal Marine Science*, 11, 151–166, 1980.
- Thorpe, S. A., Internal wave reflection and scatter from sloping rough topography, *J. Phys. Oceanogr.*, 31, 537–553, 2001.
- Webb, D. J., and N. Suginohara, Vertical mixing in the ocean, *Nature*, 409, 37–37, 2001.
- Wunsch, C., Internal tides in the ocean, *Rev. Geophys.*, 13, 167–182, 1975.

This preprint was prepared with AGU’s L^AT_EX macros v4, with the extension package ‘AGU++’ by P. W. Daly, version 1.6b from 1999/08/19.